A Multiscale Wavelet–Graph Spectral Approach for Cardiovascular Risk Assessment using Retinal Fundus Images

1st S Shrivatssan
Department of ECE, NIT Puducherry, India
ORCID: 0009-0003-5175-9025

2nd Malaya Kumar Nath
Department of ECE, NIT Puducherry, India
ORCID: 0000-0002-1959-6452

***Abstract*—Retinal fundus imaging provides important biomarkers associated with cardiovascular diseases (CVDs) as it enables direct visualization of microvascular structures. This work presents a signal processing framework for CVD prediction by integrating multiscale texture descriptors with graph-based structural modeling. The approach involves preprocessing, multiscale wavelet decomposition, and extraction of wavelet energy and autocorrelation features to capture texture and spatial dependencies. A graph-based representation is then constructed, and its spectral features are derived to model global structural relationships across scales and orientations. The proposed framework is evaluated on the China-Fundus-CIMT dataset. Results show that combining wavelet energy, autocorrelation, and graph spectral features enhances performance compared with individual feature sets, achieving a test accuracy of 0.735, recall of 0.900, F1-score of 0.772, and AUC of 0.800. The proposed framework provides a computationally efficient alternative to data-intensive deep learning-based approaches for CVD risk prediction.**

***Index Terms*—Cardiovascular diseases (CVDs), retinal fundus imaging, wavelet decomposition, autocorrelation, graph spectral analysis**

I. Introduction

Cardiovascular diseases (CVDs) remain the leading cause of mortality worldwide, accounting for a significant proportion of deaths each year [1]. As per the World Health Organization (WHO) report in 2025, CVDs caused an estimated 19.8 million deaths globally in 2022, accounting for 32% of global deaths, with 85% of these deaths resulting from heart attacks and strokes [1]. Early identification of individuals at high risk of CVD is necessary to enable timely preventive measures and reduce disease progression. Conventional CVD risk prediction models such as Framingham Risk Score (FRS) [2], SCORE [3], and QRISK2 [4] estimate CVD risk using a combination of variables including age, sex, systolic blood pressure, cholesterol levels (total and HDL), smoking status, diabetes status, and body mass index. These approaches often require clinical assessment and laboratory investigations, making large-scale population screening difficult.

Retinal fundus imaging has emerged as a promising non-invasive approach for CVD risk assessment. Since the retinal vasculature exhibits anatomical and physiological similarities with cerebral and coronary microvasculature, retinal images can reveal important information about systemic vascular health. Structural alterations in retinal vessels, such as arteriolar narrowing, venular dilation, arterio-venous nicking, vessel tortuosity, and changes in vessel calibre, have been shown to correlate with CVDs [5]. As retinal fundus photography enables rapid and cost-effective acquisition of vascular information, it offers a practical modality for large-scale CVD risk assessment.

Recent advances in artificial intelligence have enabled the automated analysis of retinal fundus images for CVD risk prediction. It has been shown that deep learning (DL) models, especially convolutional neural networks, can directly estimate cardiovascular risk factors from retinal images. For example, Poplin *et al.* demonstrated that DL models can predict systemic risk factors such as age, blood pressure, smoking status, and body mass index (BMI) from retinal images [6]. DL frameworks and multimodal approaches for CVD risk stratification using retinal images have been further explored in recent studies [8]–[10].

DL approaches have shown strong performance in extracting CVD risk features from retinal images. However, these models often require large annotated datasets and rely on computationally intensive architectures. Furthermore, their performance can be sensitive to dataset size and variations in imaging conditions. To address these limitations, recent studies have explored computational analysis of retinal images to identify biomarkers associated with cardiovascular health. Vessel calibre, vascular morphology, and texture characteristics have been shown to provide clinically relevant information while maintaining computational efficiency [12].

In this work, a signal processing-based framework is proposed for the analysis of retinal fundus images for CVD prediction. The proposed method introduces a graph-based spectral representation, complemented by wavelet energy and autocorrelation features, to characterize complex retinal image patterns. Existing handcrafted retinal studies have commonly employed vascular morphology and texture-based descriptors, including Haralick-based texture representations [14]. Haralick-based texture descriptors primarily quantify localized texture relationships and do not explicitly capture structural dependencies across multiple spatial scales. In contrast, wavelet energy captures multiscale retinal texture variations, autocorrelation characterizes spatial dependencies and repetitive vas-

cular patterns, and graph spectral features model hierarchical structural relationships within retinal vascular networks. The integration of these complementary descriptors enables a more comprehensive characterization of retinal patterns associated with CVD risk prediction.

The main contributions of this work are summarized as follows:

1) A graph-based spectral representation is used for capturing global structural relationships present in retinal image patterns.
2) Integration of complementary wavelet energy and autocorrelation features to characterize multiscale retinal texture variations.
3) Evaluation of the proposed framework on the China-Fundus-CIMT dataset using a random forest classifier for CVD risk prediction.

II. RELATED WORK

Existing approaches for CVD risk prediction from retinal fundus images can be broadly categorized into DL-based and handcrafted feature-based methods. The summary of existing approaches, along with their techniques, performance, and limitations is presented in Table I.

TABLE I: Literature review of CVD risk assessment from retinal fundus images.

Sl.No.	Author(s), year	Techniques	Performance	Limitations
1	Poplin et al., 2018	Inception-v3	AUC: * Gender-97.00. * Smoking-71.00, * MACE-70.00	* Low predictive performance for BMI & HbA1C
2	Cheung et al., 2021	CNN (SIVA-DLS)	ICC: 0.82 to 0.95	* Vulnerable to artifacts.
3	Zhang et al., 2023	Reti-WHO (Swin transformer)	R2-score = 0.503, MAE = 1.58, SEN = 0.81, SPE = 0.66.	* High false negatives.
4	Sathya & Mahesh 2025	Multimodal DL: * HRV-GT + STC-T + SMM Fusion + CHRC-Net	AUC = 97.00	* Reliance on cross-sectional data. * Limited interpretability.
5	Bisna et al., 2025	EfficientNet-B3 + clinical data fusion	ACC = 92.40 AUC = 96.30	* Required clinical validation.

Recent studies have demonstrated that DL techniques achieve strong predictive performance by learning hierarchical features directly from the retinal images to predict CVD risk [6] [7] [9] [13]. Various architectures, including CNN and transformer-based models, have been explored for CVD prediction [8] [11]. In addition, some recent studies have extended these approaches to multimodal frameworks, where clinical and demographic information is integrated with the images for improved risk stratification [10].

In parallel, feature-based methods focus on extracting clinically relevant retinal biomarkers such as, vessel calibre, structural morphology and texture characteristics. These methods employ handcrafted descriptors derived from intensity statistics and spatial relationships in the retinal images such as, gray-level co-occurrence matrix (GLCM)-based texture features, color distribution features, making them computationally efficient and easy to interpret [12]. GLCM features quantify the spatial relationship between pair of neighboring pixel intensities, thereby capturing local characteristics.

Despite this, existing DL methods exhibit certain limitations as they often require large-scale annotated datasets and significant computational resources. On the other hand, the feature-based approaches fail to capture the long-range structural dependencies and inter-scale relational patterns present in retinal vasculature because they primarily depend on localized descriptors. Therefore, there is a need for a feature-driven approach that effectively captures both the local texture information and global structural relationships in retinal fundus images for CVD risk prediction.

III. PROPOSED METHODOLOGY

The proposed method for CVD predication consists of preprocessing, wavelet energy feature extraction, autocorrelation-based analysis, graph construction, graph spectral feature extraction, and classification. The block diagram of the proposed method is shown in Fig. 1

A. PREPROCESSING

The green channel of colour fundus images from the China Fundus CIMT dataset is used as it provides highest contrast between the retinal vessels and the background. Contrast-limited adaptive histogram equalization (CLAHE) is applied to these images to improve the vessel visibility and suppress non-uniform illumination [15]. The resulting image is then normalized using min-max normalization to ensure a consistent intensity range across samples.

B. MULTISCALE WAVELET ENERGY FEATURES

A multilevel 2-D discrete wavelet transform (DWT) [16] is applied to the preprocessed image to capture the texture characteristics at different spatial resolutions. At each level of decomposition, the image is decomposed into one approximation (low frequency) subband and three detail subbands i.e., LH (horizontal), HL (vertical), and HH (diagonal). The spatial resolution of each subband decreases as level of decomposition increases and this leads to reduced number of coefficients at higher levels. This enables the analysis of both fine and coarse structural patterns present in the retinal images.

For each subband, the energy is computed as sum of squared wavelet coefficients i.e., $E_{l,b} = \sum_{i,j} W_{l,b}(i,j)^2$.

Where, $W_{l,b}(i,j)$ denotes the wavelet coefficient at level l and sub-band b. Direct comparison of energy values can be misleading as it may introduce some bias towards lower levels having large number of coefficients, so to address this limitation, a normalized energy measure is employed to ensure that energy values are independent of subband size:

$$\tilde{E}_{l,b} = \frac{1}{N_l} \sum_{i,j} W_{l,b}(i,j)^2$$

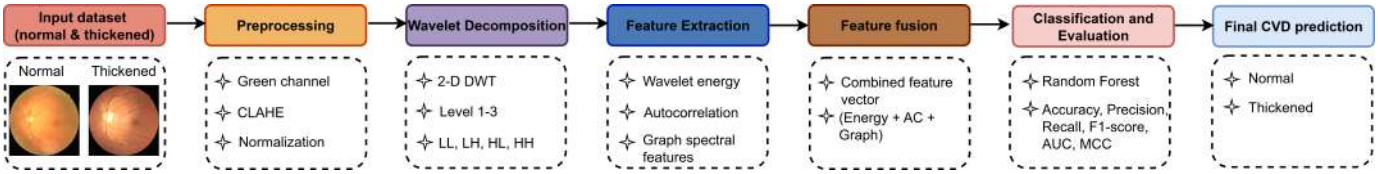

Fig. 1: Overall framework of the proposed method for CVD risk prediction from retinal fundus images.

where N_l represents the total number of coefficients in the corresponding sub-band. To further characterize the high frequency content, the total detail energy at each level is computed by combining the horizontal, vertical and diagonal components which represents the overall edge and texture strength at a given scale ($E^{(l)}_{detail} = E^l_{LH} + E^l_{HL} + E^l_{HH}$).

In addition to capture how structural information is distributed across the scales, a relative energy measure (i.e., $R_l = \frac{E^{(l)}_{detail}}{\sum_{k=1}^{L} E^{(k)}_{detail}}$). Where $L = 3$ denotes the total number of decomposition levels. This relative measure provides a scale-invariant energy representation, enabling consistent comparison across decomposition levels which highlights the relative contribution of fine and coarse structural components. However, while wavelet energy features quantify the magnitude of frequency components in each subband, they do not explicitly capture the spatial organization of structural patterns.

C. AUTOCORRELATION-BASED SPATIAL ANALYSIS

2-D autocorrelation is applied to wavelet detail subbands to capture the arrangement and persistence of vessel structures, which act as discriminative features, as different structural patterns may exhibit similar energy distributions. For each decomposition level, the detail subbands LH, HL, and HH are analyzed individually using the 2-D autocorrelation function. For a given subband, $W_{l,b}(x, y)$, the autocorrelation map is obtained by $R_{l,b}(u, v) = \sum_{x,y} W_{l,b}(x, y)W_{l,b}(x + u, y + v)$. Where, (u, v) denotes the spatial shift. The resulting map is normalized with respect to its maximum value to ensure that the representation is independent of absolute magnitude, and the normalized autocorrelation map is denoted by $\tilde{R}_{l,b}(u, v)$. For each normalized autocorrelation map, three scalar descriptors are extracted. The mean autocorrelation,

$$AC_{mean} = \frac{1}{N} \sum_{u,v} \tilde{R}_{l,b}(u, v)$$

represents the average spatial similarity across all shifts. The standard deviation,

$$AC_{std} = \sqrt{\frac{1}{N} \sum_{u,v} \left(\tilde{R}_{l,b}(u, v) - AC_{mean} \right)^2}$$

captures the variation in correlation values, indicating how structural similarity changes across the image. In addition, a decay-based descriptor is computed from the central horizontal profile of the normalized autocorrelation map

$$AC_{decay} = \frac{1}{15} \sum_{u=5}^{19} \left| \tilde{R}_{l,b}(u, 0) \right|$$

where u denotes the horizontal spatial shift from the autocorrelation center, and the shift range is fixed from 5 to 19 pixels. This range was selected empirically to reduce the influence of the central autocorrelation peak while preserving meaningful spatial dependencies. This descriptor quantifies the persistence of structural similarity at non-zero displacements, where higher values indicate better preservation of vascular organization typically associated with lower CVD risk, whereas lower values reflect faster correlation decay and greater structural irregularity often observed in CVD cases.

D. GRAPH-BASED SPECTRAL ANALYSIS

A graph-based representation is constructed using the autocorrelation descriptors obtained from different wavelet decomposition levels and sub-bands to capture the global structural relationships in fundus images associated with CVDs [17]. This explicitly models the relationships between structures across different levels and orientations, whereas the previously extracted features capture only local frequency characteristics and spatial organization. In retinal vasculature, structural characteristics vary between normal and pathological conditions, with CVDs associated with vascular abnormalities and changes in vessel morphology [5]. These variations occur across different scales and orientations. Therefore, it is important to capture how these structures relate to one another.

1) Graph Construction: Each wavelet detail subband (horizontal, vertical, diagonal) obtained from different decomposition levels is treated as a node in the graph. In a three-level decomposition, a total of nine nodes are formed corresponding to the combinations of levels and orientations i.e., (LH, HL, HH). Each node in the graph is represented using a feature vector constructed from the autocorrelation descriptors i.e., $f = [\phi_\mu, \phi_\sigma, \phi_\tau]$.

The relationships between nodes are defined based on cosine similarity of their corresponding feature vectors, which measure the pairwise relationship between nodes. Subbands exhibiting similar structural pattern produce similar autocorrelation characteristics.

$$A_{i,j} = \frac{f_i \cdot f_j}{\| f_i \| \| f_j \|}$$

The computed similarities are used to construct the adjacency matrix $A \in \mathbb{R}^{N \times N}$, where N denotes the number of nodes. A higher value of $A_{i,j}$ indicates stronger structural similarity between the corresponding subbands.

2) Graph Spectral Analysis: Spectral analysis is performed using the normalized graph Laplacian to capture the global structural properties of the constructed graph. Degree matrix

'$D_{i,i} = \sum_j A_{i,j}$' is computed from the adjacency matrix A. Where, $D_{i,j} = 0$. The normalized graph Laplacian is then defined as $L_{norm} = I - D^{-1/2} A D^{-1/2}$ [17]. Where, I denotes the identity matrix. It reduces the influence of variations in node degree. Since different subband nodes may have different connectivity strengths, normalization ensures that the spectral representation reflects relative structural relationships rather than being dominated by highly connected nodes. The eigenvalues of L_{norm}, denoted by $0 = \lambda_1 \leq \lambda_2 \leq \cdots \leq \lambda_N$, are computed, and the corresponding spectral features are extracted to characterize the structural properties of the graph. The second smallest eigenvalue λ_2, known as the algebraic connectivity is computed which reflects the overall connectivity between the subband nodes. In addition, λ_3 is included to capture higher-order variations in the spectral structure. The largest eigenvalue and the standard deviation of eigen values is computed to quantify the spread of graph spectrum. Largest eigenvalue represents the maximum variation in the graph, while the standard deviation of eigenvalues captures the variability in structural relationships across the subband nodes.

Furthermore, spectral entropy is computed from non-trivial eigenvalues to characterize the complex relationships (i.e., degree of structural disorder) within the graph. Eigenvalues are normalized (i.e., $p_i = \frac{\lambda_i}{\sum_j \lambda_j}$) to form a probability distribution. Where, $i, j \in [1, N]$. Lower entropy indicates a more organized and consistent relationship between subband nodes, whereas higher entropy corresponds to increased complexity and heterogeneity in the graph structure. In addition, the non-trivial eigenvalue spectrum is divided into low-, mid-, high-frequency bands based on ascending order of eigenvalues. The spectral energy in each band is computed as sum of eigenvalues within that band. The normalized energy ratios of these bands are computed to represent the spectral energy distribution across different frequency components. These features provide information about relative contribution of low and high frequency structural variations.

Overall, graph-based spectral analysis extracts a set of discriminative features that capture the structural organization of relationships between wavelet subbands using autocorrelation-based features. The constructed graph captures the structural similarities between subbands, and its spectral analysis provides a compact representation of global structural organization. The extracted spectral descriptors, including λ_2 (connectivity), λ_3, largest eigenvalue, standard deviation of eigenvalues, spectral entropy, and band energy distribution capture the variations in inter-scale structural relationships.

E. FEATURE INTEGRATION AND CLASSIFICATION

The final feature representation is obtained by combining the wavelet energy features, autocorrelation-based descriptors, and graph-spectral features into a unified feature vector for each retinal image. The wavelet energy features capture multiscale local frequency characteristics, autocorrelation features describes spatial dependencies, and graph spectral features model global structural relationships across scales and orientations. These features are then used for classification to distinguish between normal and pathological cases associated with CVDs. Random forest is employed for classification because of its ability to handle high-dimensional feature spaces and capture non-linear relationships. Additionally, it does not require strict feature scaling and works well with the proposed feature set. The random forest classifier was implemented using scikit-learn version 1.7.2 with 300 decision trees, a maximum depth of 8, a minimum leaf size of 5, balanced class weighting, and a fixed random seed of 42 to ensure reproducibility.

IV. RESULTS AND DISCUSSIONS

The proposed approach illustrated in Fig. 1 is applied to the retinal images from the China-Fundus-CIMT dataset, and the results are presented in Table II. The dataset description is provided below, and performance of the proposed framework is evaluated using accuracy, precision, recall, F1-score, AUC, and MCC. For brevity, E, AC, and GS denote wavelet energy, autocorrelation, and graph spectral features, respectively.

TABLE II: Performance comparison of the proposed feature configurations and fundus-only DL baselines.

Method	**Acc**	**Prec**	**Rec**	**F1**	**AUC**	**MCC**
E	0.650	0.621	0.770	0.687	0.727	0.309
E + AC	0.720	0.672	0.860	0.754	0.798	0.458
E + AC + GS (**Proposed**)	0.735	0.677	**0.900**	0.772	0.800	0.498
DenseNet121	0.740	0.700	0.840	0.764	0.842	0.490
EfficientNet-B0	0.780	0.769	0.800	0.784	0.840	0.560

A. DATASET

The proposed approach was evaluated on the China Fundus-CIMT dataset [18], which consists of bilateral high-resolution retinal fundus images acquired from 2,903 patients. Each subject underwent retinal imaging and carotid ultrasound examination, during which carotid intima-media thickness (CIMT) was measured. Based on the CIMT values, the images were categorized into two groups: normal (CIMT < 0.9 mm) and thickened (CIMT ≥ 0.9 mm). The dataset was divided into training, validation, and test sets using a patient-wise split to prevent data leakage. This resulted in 5,206, 400, and 200 retinal images for the training, validation, and test sets, respectively. The corresponding normal/thickened class distributions were 1398/3808, 200/200, and 100/100, and no patient appeared in more than one subset.

B. RESULTS

The performance of the proposed framework is evaluated using a random forest classifier across three feature configurations: wavelet energy only, wavelet energy with autocorrelation, and the complete feature set. The energy-only configuration achieved an accuracy of 0.650 and an AUC of 0.727, indicating that basic multiscale texture information provides limited discriminative capability for CVD risk prediction. The addition of autocorrelation features improved the performance,

achieving a test accuracy of 0.720 and an AUC of 0.798. This improvement highlights the importance of extracting spatial dependencies and structural patterns present in retinal vasculature. Further improvement was observed when graph spectral features were incorporated, where the proposed framework achieved the best performance among the handcrafted feature configurations, with a test accuracy of 0.735, F1-score of 0.772, AUC of 0.800, and MCC of 0.498. This demonstrates that modeling inter-scale and orientation relationships using graph-spectral analysis provides additional discriminative information that is not captured by local features alone. The progressive improvement from the energy-only configuration to E+AC and subsequently to E+AC+GS suggests that autocorrelation features contribute substantially to the performance gain, while graph spectral descriptors provide complementary discriminative information that further enhances classification performance. In comparison, the fundus-only DL baselines, DenseNet121 and EfficientNet-B0, were trained and evaluated using the same preprocessing pipeline and patient-wise dataset split to ensure a fair comparison under identical experimental conditions. Although these models achieved higher overall accuracy and F1-score, the proposed framework attained the highest recall (0.900), indicating an enhanced ability to identify high-risk CVD patients. This improved sensitivity reduces the likelihood of missing positive cases and may therefore be advantageous in screening applications requiring early risk detection and timely clinical intervention. Moreover, the proposed framework relies on computationally efficient handcrafted descriptors and a lightweight random forest classifier, making it suitable for deployment in settings with limited data availability and computational resources.

To further assess the robustness of the proposed feature representation, additional experiments were conducted using support vector machine (SVM) with a radial basis function (RBF) kernel and XGBoost under the same experimental settings. Although the relative performance varied across classifiers, random forest achieved the best overall performance among the evaluated ML classifiers, demonstrating its suitability for modeling heterogeneous feature representations.

V. Conclusions

In this work, a feature-driven framework for CVD risk prediction from retinal fundus images is proposed. This framework combines multiscale wavelet energy features, autocorrelation-based spatial descriptors, and graph spectral features to effectively capture local texture information, spatial dependencies, and global structural relationships in retinal vasculature. Experimental results show that progressively incorporating autocorrelation and graph spectral features improves classification performance over the individual handcrafted feature configurations, as reflected by higher accuracy, F1-score, AUC, and MCC, while attaining a recall of 0.900 for identifying high-risk CVD patients. This high sensitivity reduces the likelihood of missing positive cases and may therefore be advantageous in screening applications requiring early risk detection and timely clinical intervention. The proposed framework offers a computationally efficient feature-based alternative for CVD risk prediction by leveraging structured representations derived from retinal images. By integrating multiscale signal characteristics with spatial and relational information, the proposed framework captures underlying vascular patterns associated with CVDs. Furthermore, its lightweight design makes it well suited for deployment in settings with limited data availability and computational resources.

References

[1] World Health Organization, "Cardiovascular diseases (CVDs)," WHO, 2025. [Online]. Available: https://www.who.int/news-room/fact-sheets/detail/cardiovascular-diseases-(cvds)

[2] R. B. D'Agostino *et al.*, "General cardiovascular risk profile for use in primary care: The Framingham Heart Study," *Circulation*, vol. 117, no. 6, pp. 743–753, Feb. 2008.

[3] R. M. Conroy *et al.*, "Estimation of ten-year risk of fatal cardiovascular disease in Europe: The SCORE project," *Eur. Heart J.*, vol. 24, no. 11, pp. 987–1003, Jun. 2003.

[4] J. Hippisley-Cox *et al.*, "Predicting cardiovascular risk in England and Wales: Prospective derivation and validation of QRISK2," *BMJ*, vol. 336, no. 7659, pp. 1475–1482, Jun. 2008.

[5] T. Y. Wong *et al.*, "Retinal arteriolar narrowing and risk of coronary heart disease in men and women. The Atherosclerosis Risk in Communities Study," *JAMA*, vol. 287, no. 9, pp. 1153–1159, Mar. 2002.

[6] R. Poplin *et al.*, "Prediction of cardiovascular risk factors from retinal fundus photographs via deep learning," *Nat. Biomed. Eng.*, vol. 2, pp. 158–164, Feb. 2018.

[7] Z. Lin *et al.*, "Addressing underestimation and explanation of retinal fundus photo-based cardiovascular disease risk score: Algorithm development and validation," *Comput. Biol. Med.*, vol. 189, Art. no. 109941, May 2025.

[8] N. D. Bisna, P. Sona, and A. James, "Retinal image analysis for heart disease risk prediction: A deep learning approach," *IEEE Access*, early access, Jan. 2025.

[9] R. M. W. Tseng *et al.*, "Validation of a deep-learning-based retinal biomarker (Reti-CVD) in the prediction of cardiovascular disease: Data from UK Biobank," *BMC Med.*, vol. 21, no. 1, Art. no. 28, Jan. 2023.

[10] Y. C. Lee *et al.*, "Multimodal deep learning of fundus abnormalities and traditional risk factors for cardiovascular risk prediction," *npj Digit. Med.*, vol. 6, no. 1, Art. no. 14, Feb. 2023.

[11] W. Zhang, Z. Tian, F. Song, P. Xu, D. Shi, and M. He, "Enhancing stability in cardiovascular disease risk prediction: A deep learning approach leveraging retinal images," *Inform. Med. Unlocked*, vol. 42, Art. no. 101366, Sept. 2023.

[12] C. Y. Cheung *et al.*, "A deep-learning system for the assessment of cardiovascular disease risk via the measurement of retinal-vessel calibre," *Nat. Biomed. Eng.*, vol. 5, no. 6, pp. 498–508, Jun. 2021.

[13] K. Sathya and G. Magesh, "Multimodal deep learning for cardiovascular risk stratification: Integrating retinal biomarkers and cardiovascular signals for enhanced heart attack prediction," *IEEE Access*, early access, Jan. 2025.

[14] O. Sijilmassi, "Non-Invasive Retinal Pathology Assessment Using Haralick-Based Vascular Texture and Global Fundus Color Distribution Analysis," *J. Imaging*, vol. 11, no. 9, Art. no. 321, Sept. 2025.

[15] K. J. Zuiderveld, "Contrast Limited Adaptive Histogram Equalization," in *Graphics Gems IV*, P. S. Heckbert, Ed. San Diego, CA, USA: Academic Press, 1994, pp. 474–485.

[16] S. G. Mallat, "A theory for multiresolution signal decomposition: The wavelet representation," *IEEE Trans. Pattern Anal. Mach. Intell.*, vol. 11, no. 7, pp. 674–693, Jul. 1989.

[17] D. I. Shuman, S. K. Narang, P. Frossard, A. Ortega, and P. Vandergheynst, "The emerging field of signal processing on graphs: Extending high-dimensional data analysis to networks and other irregular domains," *IEEE Signal Process. Mag.*, vol. 30, no. 3, pp. 83–98, May 2013.

[18] N. Guo *et al.*, "High-resolution fundus images for ophthalmomics and early cardiovascular disease prediction," *Sci. Data*, vol. 12, no. 1, Art. no. 568, Apr. 2025.